Applied Physics A (2019) 125:535
https://doi.org/10.1007/s00339-019-2844-x

**Applied Physics A**
**Materials Science & Processing**

# Mechanically tunable single-component soft polydimethylsiloxane (PDMS)-based robust and sticky superhydrophobic surfaces

**Pritam Kumar Roy[1] · Sanjeev Kumar Ujjain[1] · Sneha Dattatreya[1] · Sumana Kumar[1] · Reeta Pant[1] · Krishnacharya Khare[1]**

Received: 1 March 2019 / Accepted: 17 July 2019 / Published online: 22 July 2019


**Abstract**
In this letter, we report the fabrication of robust and mechanically tunable superhydrophobic surfaces based on elastic wrinkles having bi-modal distribution of roughness. Contrary to most superhydrophobic surfaces, where different nano- and/or micro-scale materials are used to create hierarchical roughness, we create them in the same material as of the substrate. Primary roughness is due to the micron-sized one-dimensional wrinkles while a nanoscale secondary roughness is created on top of the wrinkles using replica molding through a nano-master. Due to the elastic nature of the underneath polymer, polydimethylsiloxane (PDMS), the fabricated superhydrophobic wrinkles demonstrate mechanically tunable wetting behavior between superhydrophobic and hydrophobic states. Water drops depict sticky superhydrophobic behavior on the fabricated samples as they show the Cassie impregnated state corresponding to the Petal effect.

## 1 Introduction

Manipulation of surface wettability using external stimuli has been an exciting area of research as it has potential applications in various areas including microfluidics, controlled drug delivery, molecular recognition, cell attachment, chemical sensing to name a few [1–5]. Wetting behavior of a solid surface primarily depends on its surface energy and surface heterogeneity (chemical or topographical) [6]. It can be tuned by varying surface energy using a suitable material, e.g., silane, perfluoro polymer, etc., or modifying the surface roughness or combination of both [7–11]. An appropriate combination of surface energy (coating) and roughness is required to demonstrate superhydrophobic behavior on a solid surface where the water contact angle can be as high as 165° [12–19]. Due to high contact angle and low-contact angle hysteresis, water drops form minimum contact area with the solid surface and hence move easily upon tilting or vibrating the surface. Nature presents two types of superhydrophobic surfaces, low adhesion superhydrophobic surfaces ('Lotus effect' corresponding to Cassie–Baxter wetting state) and high adhesion superhydrophobic surfaces ('Petal effect' corresponding to Cassie impregnating wetting state) [17, 20–30]. Although both types of superhydrophobic surfaces show similar values of water contact angles, they show completely opposite adhesion behavior of water drops. In spite of completely different characteristics, both types of superhydrophobic surfaces have been found useful in various applications hence are still an active topic for research [20, 21, 28, 31, 32]. Superhydrophobicity, being a surface phenomenon, is very sensitive to surface damage. Most superhydrophobic surfaces, including lotus leaves, lose their superhydrophobic characteristics upon mechanical or chemical damage. Recently, many researchers have attempted to fabricate mechanically chemically and environmentally stable superhydrophobic surfaces which are very useful in applications such as oil–water separation, non-wetting fabrics, anti-corrosion, anti-icing, etc. [33–39].

Surface wettability of solid surfaces can be actively and reversibly manipulated using a smart responsive material with proper external stimuli, e.g., mechanical strain, electric field, temperature, pH, UV light, etc. [14, 40–46]. Various research groups have demonstrated reversible switching between two different wetting states (from hydrophobic to hydrophilic or superhydrophobic

**Electronic supplementary material** The online version of this article (https://doi.org/10.1007/s00339-019-2844-x) contains supplementary material, which is available to authorized users.

✉ Krishnacharya Khare
kcharya@iitk.ac.in

[1] Department of Physics, Indian Institute of Technology Kanpur, Kanpur 208016, India

to superhydrophilic) using one of the above-mentioned stimuli. Out of these, mechanical strain-controlled switching of surface wettability is of particular importance as there are no strict conditions in choosing various components. Elastic wrinkles on PDMS are one of the best candidates to demonstrate mechanical strain-controlled wetting behavior because of its low cost, easy preparation, non-toxicity, optical transparency and mechanically robust nature [41, 46–49]. Due to the elastic nature of PDMS, the topography of wrinkle pattern can be manipulated upon applying external strain, hence the resulting wetting behavior also gets affected. With appropriate surface engineering, wrinkle surfaces can demonstrate any wetting state between superhydrophobic and superhydrophilic [41, 47]. Mangialardi et al. and Yang et al. showed that only micron-scale PDMS-based wrinkles cannot demonstrate superhydrophobic behavior [41, 50]. Therefore, the introduction of nanoscale roughness on micron-scale wrinkle surface is essential to achieve superhydrophobicity. Lin et al. introduced functionalized silica nanoparticles on wrinkle surface to achieve dual-scale roughness hence superhydrophobicity [41]. They calculated that only micron-sized wrinkles would show superhydrophobic behavior if $\frac{A}{\lambda} < \frac{\tan\theta_Y}{-2\pi}$, where $A$ and $\lambda$ are amplitude and wavelength of wrinkle pattern, respectively, and $\theta_Y$ is the Young's contact angle on the planar surface. Therefore, to achieve superhydrophobicity with only wrinkle pattern, one should fabricate wrinkles with about 150% pre-strain which is not possible for PDMS as it cannot withstand strain beyond 80%. Therefore, they used functionalized nanoparticles to increase the apparent contact angle of PDMS sheets. However, due to poor adhesion of nanoparticles on wrinkle surface, stability of superhydrophobic behavior would be very poor. This is due to the fact that both micron-scale and nanoscale roughness are due to two difference types of materials which limits their mechanical stability. Thus, robustness and wetting tunability are two important challenges for wide-range applications of superhydrophobic surfaces and combining both these features in a same material/surface would be very beneficial from fundamental as well as application point of view.

In this article, we address the two important challenges, robustness and wetting tunability, by preparing superhydrophobic surfaces using elastic wrinkles using single-phase material. One-dimensional micron-size wrinkles were prepared on a thin PDMS sheet by exploiting the buckling instability. On top of these micron-sized wrinkles, nanoscale roughness was introduced through replica molding from a nano-master. The overall dual-scale roughness provided superhydrophobic behavior. Due to the elastic nature of wrinkles, wetting behavior of dual-scale wrinkles could be mechanically tuned between superhydrophobic to hydrophobic states.

## 2 Experimental section

### 2.1 Materials

Polydimethylsiloxane (Sylgard 184) pre-polymer and its thermal curing agent were obtained from Dow Corning Corp. Sodium borohydride ($NaBH_4$), silver nitrate ($AgNO_3$), sulfuric acid ($H_2SO_4$), hydrogen peroxide ($H_2O_2$) were of analytical grade and purchased from Sigma Aldrich India. Acetone, isopropanol and ethanol were procured from Merck, India. Single-crystal silicon (p-type) was used to create nanoscale pattern by chemical etching.

### 2.2 Characterization

Optical microscope (BX51, Olympus) and field-emission scanning electron microscope (FESEM: JEOL, JXA-8230) [accelerating voltage: 10–18 kV, beam current: 25 μA, gold-coating thickness: 8 (±3) nm] was used to analyze the surface morphology of the fabricated samples. Atomic force microscope (AFM: Park system XE-70) in a tapping mode and NanoMap-D: Dual Mode—optical and stylus 3D surface profilometer was utilized for rms surface roughness study. Static ($\theta$), advancing ($\theta_A$) and receding ($\theta_R$) contact angles were measured using Milli-Q water (resistivity 17.8 MΩ cm at 25 °C) at room temperature with a Contact Angle Goniometer (OCA35, DataPhysics, Germany). Contact angles were measured using the Laplace–Young fitting model of a 2-μL water droplet placed on a horizontal substrate. Advancing and receding contact angles were measured by first increasing the volume of a drop from 2 to 10 μL in the step of 2 μL followed by decreasing the drop volume back to 2 μL with the same step size. The difference between advancing and receding contact angles provides the contact angle hysteresis (CAH) ($\theta_A - \theta_R$). To estimate an error in a measurement, five measurements were performed at three different positions of different samples.

### 2.3 Preparation of nanostructured silicon surfaces

Silicon substrates (4 cm × 4 cm) were cleaned by ultrasonication first in acetone and then in isopropanol for 10 min followed by rinsing with de-ionized water. The cleaned substrates were then immersed in piranha solution (1:1 of concentrated $H_2SO_4$:30% w/w $H_2O_2$ in water) for 20 min at 80 °C, then thoroughly rinsed with hot (80 °C) de-ionized (DI) water. The cleaned silicon samples were etched chemically in an aqueous solution of 2 M $NaBF_4$ and 0.02 M $AgNO_3$. The etched samples were thoroughly rinsed with DI water and then immersed in 50% w/w aqueous solution of HCl and $HNO_3$ for overnight at room temperature to remove

the silver nanoparticles and dendrites deposited on the surface during the chemical etching [51]. Prepared samples were used as nano-master for the replica molding.

### 2.4 Preparation of nano- and micro-patterns on PDMS sheets

PDMS pre-polymer and curing agent (weight ratio of 10:1) were thoroughly mixed and degassed under vacuum ($10^{-2}$ Torr) in a desiccator for 30 min to remove trapped air bubbles. After that, the PDMS/curing agent mixture was poured on a nano-master and cured thermally for 3 h at 65 °C. The solidified PDMS was then carefully peeled-off from the nano-master. This PDMS sheet, with negative nanoroughness of the master pattern, was used as a substrate for preparing wrinkles.

The nanostructure PDMS sheets were cut into rectangular shape (3 cm × 1 cm) and stretched with one directional mechanical pre-strain ($\varepsilon_0$) of 60% using a custom-made stretching device. The stretched PDMS sheets were exposed to UV-ozone (144AX, Jelight Company, USA) at room temperature for 1 h (Mercury-Quartz lamps with wavelength: 254 nm, flux: 28 mW/cm$^2$, sample distance from the lamps: 2.5 cm). UV-ozone exposure oxidizes the top surface of the PDMS sheets by converting the siloxane molecules into $SiO_x$ [52]. Subsequently, the strain of the stretched oxidized samples was released very slowly (0.1 mm per second) resulting into one-dimensional wrinkle pattern. These wrinkles had oxidized PDMS surface and also the negative structure of the nano-master pattern. To overcome this, another replica of the above-generated wrinkles was taken, first by grafting the self-assembled monolayer (SAM) of fluorinated silane (heptadecafluoro-1,1,2,2-tetrahydrodecyl-dimethylchlorosilane) molecules by vapor deposition on the oxidized PDMS wrinkles followed by pouring the PDMS and curing agent mixture and crosslinking [53]. The fabrication process is schematically shown in Fig. 1.

## 3 Results and discussion

Figure 2a–c shows optical microscope, electron microscope and 3D optical profilometer images of PDMS-based wrinkles having wavelength ($\lambda$) about 50 µm and amplitude ($A$) about 11.5 µm. The optical and electron microscopy images shown in Fig. 2d, e demonstrate the surface morphology of the nano-master pattern with rms roughness about 113 nm as obtained using an AFM (cf. Fig. 2f). Figure 2g–i shows optical, SEM and 3D optical profilometer images of nanostructured PDMS surface obtained by replica molding through the nano-master. rms roughness of the nanostructured PDMS surface was about 121 nm which is similar to the roughness of the nano-master pattern. This nanostructured PDMS sheet was used to fabricate wrinkle having dual-scale roughness and their morphology is shown in Fig. 2j–l as optical, SEM and 3D optical profilometer images.

It is clear from the morphology images that the surface of these wrinkles has dual-scale roughness: micron scale due to wrinkle morphology and nanoscale due to the pattern transferred from the nano-master. rms roughness of such dual-scale wrinkles was found to be about 5.78 µm compared to the original wrinkles with 5.52 µm. Therefore, it is clear that the introduction of nanoscale roughness does not change the surface roughness by large amount.

As prepared wrinkles (after UV-ozone exposure) were found hydrophilic in nature due to the oxidized PDMS surface. Replica of such hydrophilic wrinkles were found hydrophobic due to siloxane groups of PDMS. The hydrophilic wrinkles show anisotropic wetting behavior with elongated or non-circular shape of a water drop due to underlying one-dimensional wrinkle pattern as shown in Fig. 3a.

The anisotropic wetting behavior of such wrinkles is characterized with two different contact angles along two different directions: parallel contact angle ($\theta_{\parallel}$) when contact angle is measured perpendicular to the wrinkles (or contact lines are parallel to the wrinkles) and perpendicular contact angle ($\theta_{\perp}$) when contact angle is measured parallel to the

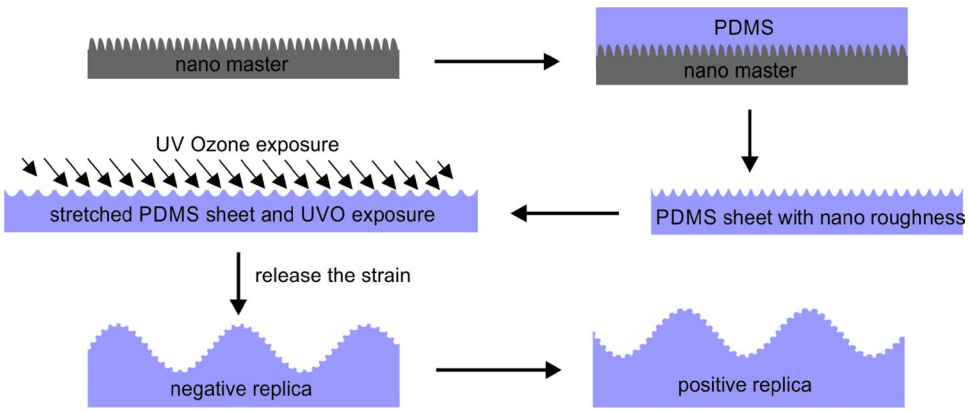


**Fig. 1** Schematic representation of the procedure for the fabrication of hierarchical patterns on PDMS substrate using replica molding technique followed by application of external mechanical strain

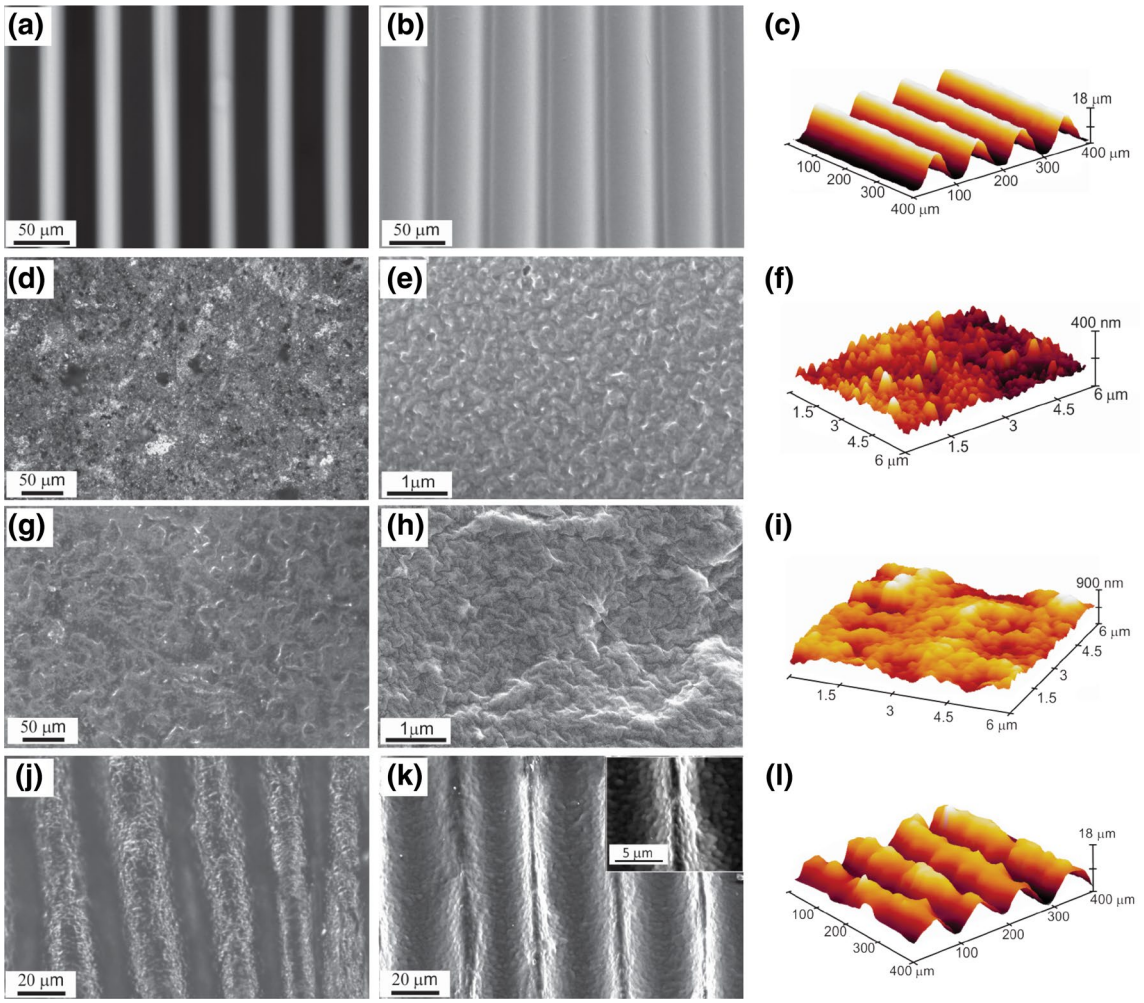


**Fig. 2** **a**, **d**, **g**, **j** Optical images of a wrinkle surface, nano-master, nano-master replica on PDMS and wrinkle with dual-scale roughness, respectively. **b**, **e**, **h**, **k** and **c**, **f**, **i**, **l** corresponding SEM and 3D optical profilometer

wrinkles (or contact lines are perpendicular to the wrinkles). Figure 3b, c shows optical images of a water drop on a wrinkle surface to measure contact angles with $\theta_{\parallel}$ and $\theta_{\perp}$ as 52° and 72°, respectively. Although PDMS is a hydrophobic material, this value of contact angle corresponds to slight hydrophobic recovery of oxidized PDMS wrinkles after UV-ozone exposure. For completely hydrophilic wrinkles (immediately after UV-ozone exposure), when a water drop is deposited, it starts flowing spontaneously into the grooves of the wrinkles due to the capillary effect as shown by Khare et al. [48]. On a wrinkle surface, the value of $\theta_{\perp}$ is found always larger than the value of $\theta_{\parallel}$. This is due to the fact that $\theta_{\parallel}$ corresponds to the Young's contact angle of the surface since the three-phase contact line of the drop is free to move parallel to the wrinkles. On the other hand, $\theta_{\perp}$ corresponds to the pinned contact angle as the three-phase contact line gets pinned perpendicular to the wrinkles. Pinning of the three-phase contact line can be at any place on a wrinkle surface and not necessary at the crest or trough of the wrinkles. Supporting movie MovieS1 shows the parallel contact angle of a water drop when the volume of the drop is increased. It is clear from the movie that the parallel contact angle remains almost the same since the three-phase contact line moves upon increasing the drop volume. Similar behavior of smooth contact line motion is observed when the drop volume is decreased. Supporting MovieS2 shows the perpendicular contact angle of a water drop with increasing drop volume. Due to pinning of the three-phase contact line in a direction perpendicular to wrinkles, the contact angle does not remain constant, rather increases, while the drop volume is increased. Upon decreasing the drop volume, the three-phase contact line remains pinned resulting in much lower contact angle at the end.

Due to the elastic nature of the wrinkles, surface topography of a wrinkle pattern can be reversibly tuned on the application of external strain. Jiang et al. analytically calculated

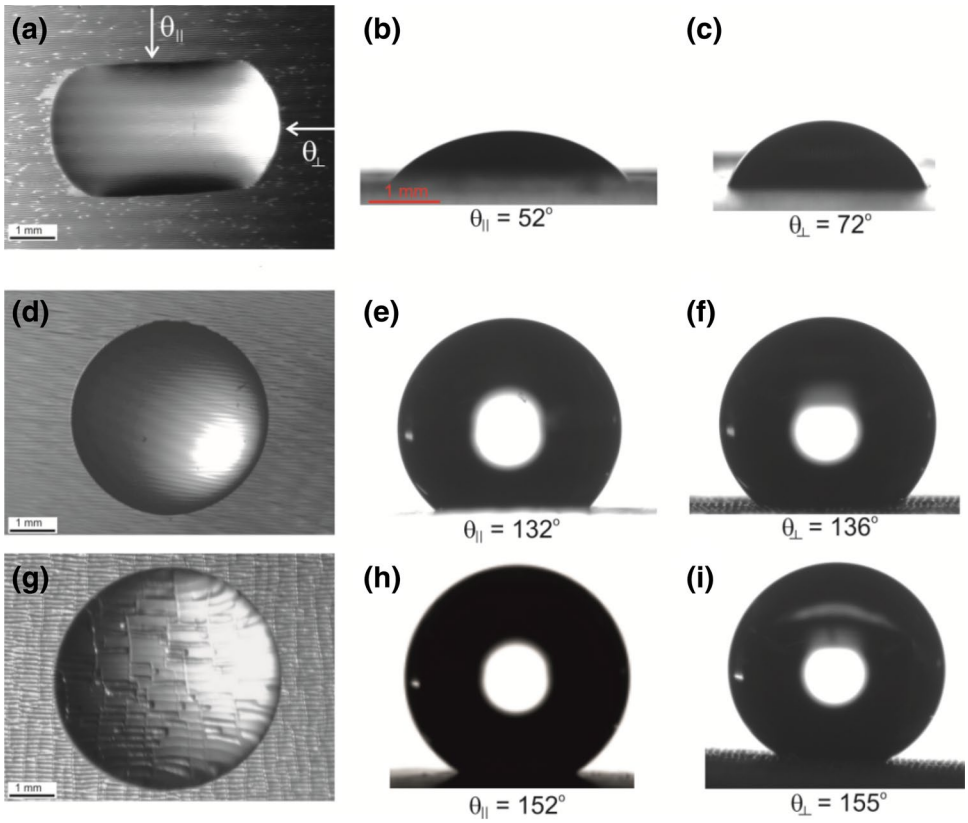


**Fig. 3** **a**, **d**, **g** The top views of water drops on hydrophilic, hydrophobic and superhydrophobic wrinkle surfaces, respectively, with anisotropic drop shape and circular drop shapes with 132° and 152° contact angles, respectively. **b**, **c**, **e**, **f**, **h**, **i** The optical images of a water drop to measure contact angles in parallel and perpendicular directions on the hydrophilic, hydrophobic and superhydrophobic wrinkle surfaces, respectively

the wavelength and amplitude of wrinkles as a function of external strain which is given as:

$$\lambda = \frac{\lambda_0(1+\varepsilon)}{(1+\varepsilon_0)(1+\varepsilon+\zeta)^{1/3}} \quad \text{and} \quad A = \frac{t\sqrt{\frac{(\varepsilon_0-\varepsilon)}{\varepsilon_c}-1}}{\sqrt{(1+\varepsilon_0)}(1+\varepsilon+\zeta)^{1/3}}, \tag{1}$$

where as $\lambda_0 = 2\pi t\left(\bar{E}_f/3\bar{E}_s\right)^{1/3}$, $A_0 = t\left(\left(\varepsilon_0/\varepsilon_c\right)-1\right)^{1/2}$, $\varepsilon_0$ is pre-strain, $\varepsilon$ is applied strain, $\varepsilon_c\left(=-1/4\left(3\bar{E}_s/\bar{E}_f\right)^{2/3}\right)$ is critical strain, $\bar{E}=\left(E/1-\nu^2\right)$, $E$ is elastic modulus, $\nu$ is Poisson's ratio, $\zeta = \frac{5}{32}\left(\varepsilon_0-\varepsilon\right)\left(1+\varepsilon_0\right)$, f and s represent film and substrate, respectively [49, 54, 55]. Therefore, the anisotropic wetting behavior can also be reversibly tuned on such wrinkle surface with applied strain. Supporting video MovieS3 shows how an elongated (anisotropic) drop shape on a wrinkle surface changes to a circular (isotropic) one if the wrinkle surface is stretched. This change of a drop shape is also reversible similar to stretching of a wrinkle surface.

To increase the hydrophobic behavior of the wrinkle surface, as prepared hydrophilic wrinkles were replicated in fresh PDMS. The replicated wrinkles had the same topography as the original wrinkles but were hydrophobic in nature. Wetting behavior of replicated hydrophobic wrinkles was found quite different compared to the hydrophilic wrinkles. Water drops on such hydrophobic wrinkles do not show anisotropic or non-circular shape even though they experience similar linear or one-dimensional wrinkle pattern underneath them. Figure 3d shows top view of a water drop on a hydrophobic wrinkle surface with almost circular three-phase contact line. Due to the circular shape, contact angles of the drop along parallel and perpendicular directions was also quite similar with values of $\theta_{\parallel}$ and $\theta_{\perp}$ to be 132° and 136°, respectively (Fig. 3e, f). The almost equal values of the two different contact angles also confirm the circular shape of a water drop on the wrinkle surface. Similar to hydrophobic wrinkles, water drops showed completely circular shape on wrinkles with dual-scale roughness as shown in Fig. 3g. Due to the presence of additional nanoscale roughness on top of the micron-scale wrinkles, these dual-scale wrinkles show superhydrophobic behavior. Water drops on such superhydrophobic wrinkles show almost the same value of contact angles in parallel and perpendicular directions as 152° and 155°, respectively as shown in Fig. 3h, i.

Before investigating the static and tunable wetting behavior of dual-scale superhydrophobic wrinkles, static wetting behavior of only micron-sized linear wrinkles were analyzed. Static contact angle and contact angle hysteresis on a hydrophobic wrinkle surface was also analyzed as a function of applied strain. As discussed earlier, the elastic wrinkles show mechanically tunable topography. Figure 4a

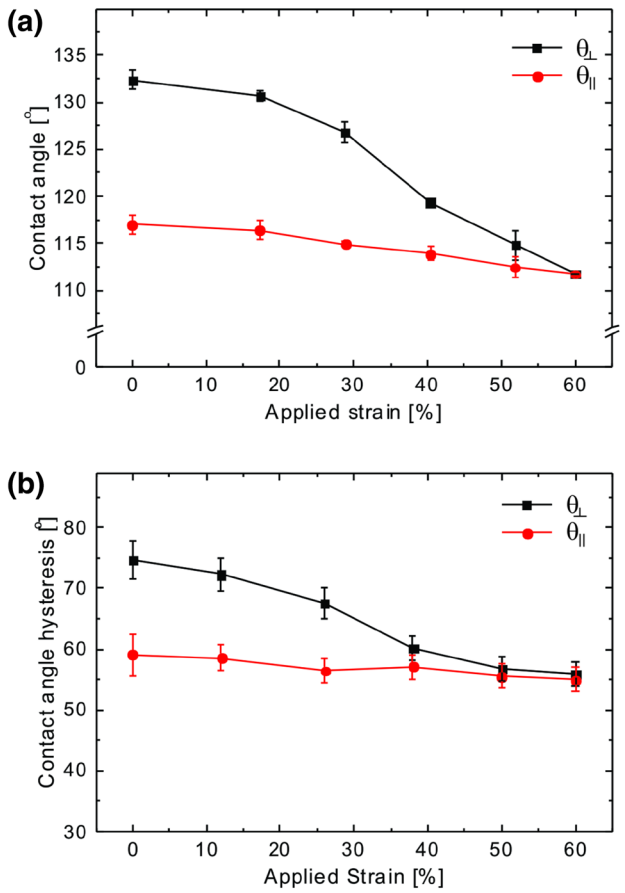


**Fig. 4** Variation of **a** water contact angle and **b** contact angle hysteresis as a function of applied mechanical strain in the perpendicular (black data points) and parallel (red data points) directions on a hydrophobic wrinkles surface (only micron-size wrinkles)

shows the variation of contact angle in perpendicular (black data points) and parallel (red data points) directions as a function of applied strain. It is clear from the graph that the perpendicular and parallel contact angles decrease monotonically from 132° to 110° and 128° to 110°, respectively upon applying the maximum 60% strain which corresponds to almost flat surface. At 0% strain, wrinkles have maximum amplitude and a water drop sitting on a wrinkle surface stay in the Wenzel state. Wenzel roughness factor ($r$) for a sinusoidal geometry can be calculated using the following eqaution:

$$r = \frac{4\pi A}{\lambda R^2} \int_0^R \left( \frac{\lambda^2 x^2}{4\pi^2 A^2} + x^2 \sin^2 \frac{2\pi x}{\lambda} \right)^{1/2} \mathrm{d}x, \tag{2}$$

where $R$ is the radius of water drop sitting on a wrinkle surface and $x$ is the variable along the direction perpendicular to wrinkles [47]. For the present wrinkle system, the Wenzel roughness factor comes as 1.49 which suggests the Wenzel contact angle on the wrinkle surface as 130° which is very close to the experimental value of 132°. This confirms that water drops on a wrinkle surface stay in the Wenzel wetting state. With increasing the strain, the wrinkle amplitude decreases, which subsequently decreases the Wenzel roughness factor hence the perpendicular contact angle also decreases. At 60%, both perpendicular and parallel contact angles become equal to each other which also corresponds to the Young's contact angle on flat PDMS surface.

As the apparent contact angle on a wrinkle surface depends upon the applied strain, contact angle hysteresis also depends upon the applied strain which is shown in Fig. 4b. The contact angle hysteresis in perpendicular direction decreases monotonically with increasing strain whereas it remains almost constant in the parallel direction. This is again due to the fact that the wrinkle amplitude, hence the surface roughness, decreases in the perpendicular direction with applied strain. In parallel direction, the three-phase contact line does not experience any obstacle hence the contact angle hysteresis is independent of the applied strain.

Water contact angle on a PDMS surface having nanoscale roughness was found to be 125º compared to 115º on a flat smooth sheet. Wrinkles prepared with such nanostructured PDMS sheets show superhydrophobic behavior with as 152° and 155° contact angles in parallel and perpendicular directions, respectively, as shown in Fig. 3h, i. Due to high contact angles, wrinkle surfaces do not show anisotropic wetting behavior as the difference between perpendicular and parallel contact angles is negligible. Mechanically tunable wetting behavior of dual-scale wrinkles is shown in Fig. 5.

At 0% strain, the surface has dual-scale roughness, as a result good superhydrophobic behavior is observed with 155° and 152° contact angles in the perpendicular and parallel directions, respectively. As the applied strain is increased, wrinkle amplitude starts decreasing as shown by the optical images (dark field mode) of the wrinkle in Fig. 5b. As a result, water contact angle also starts decreasing in both directions. At 60% applied strain, the wrinkle surface becomes almost flat and only nanoscale roughness is present on the surface. Water contact angle on such 60% stretched sample becomes 128°, which is almost equal to the water contact angle on freshly prepared nanostructured PDMS sheet from replicating through the nano-master (blue data point in Fig. 5a). Dark-field optical images shown in Fig. 5b also shows that that the amplitude of wrinkle pattern decreases with increasing applied strain and for 60% case, the surface possess only nanoscale roughness as the wrinkle pattern is hardly visible. Water drops roll easily on conventional superhydrophobic surfaces upon tilting by a small angle (~2°), whereas on the dual-scale PDMS wrinkles, they exhibit highly sticky behavior. Water drops on such dual-scale PDMS wrinkles do not move even if they are tilted by 180° (upside down). Figure 6a, b shows water drops on the fabricated surface at tilt angles of 75° and 180°, respectively.

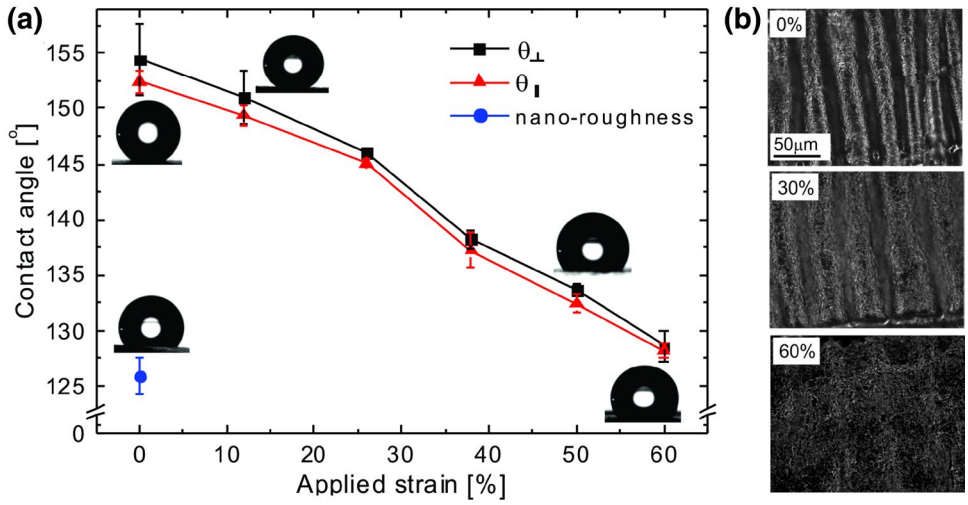


**Fig. 5** **a** Variation of water contact angle as a function of applied mechanical strain in the perpendicular (black data points) and parallel (red data points) of the wrinkles (on dual-scale roughness) and blue data point shows contact angle on positive replica of nano-master. **b** SEM micrographs of dual-scale rough wrinkles which illustrate different amplitude at different applied strain

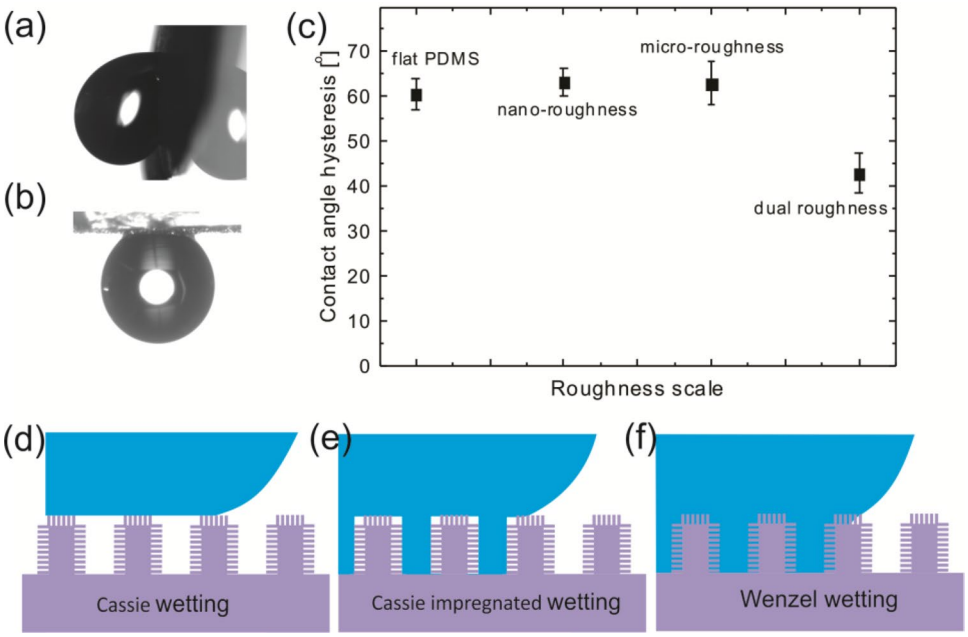


**Fig. 6** **a**, **b** Water drops on dual-scale wrinkles put at a tilt angle 75° and inverted position, respectively. **c** Contact angle hysteresis on the PDMS samples having different scale roughness. **d–f** Schematic images of Cassie, Cassie impregnating and Wenzel states

The sticky behavior of water drops can also be characterized in terms of the contact angle hysteresis. Figure 6c shows contact angle hysteresis for water on flat, nanostructured, only micron-scale wrinkle and dual-scale wrinkle surfaces which indicates that the contact angle hysteresis on all surfaces is quite high. This is due to the high adhesive nature of PDMS and Cassie-impregnating wetting behavior. According to the definition, Cassie state is a completely non-wetting state where a water drop sits on a composite surface made with solid and air. But in the Cassie impregnating wetting state, grooves or micron-scale rough areas are completely or partially wetted by a liquid but the nanoscale rough areas remain non-wetted or dry [24]. Figure 6d–f shows the schematics of the Cassie, Cassie impregnating and Wenzel states. Furthermore, the sticky nature of these surfaces is quantified by measuring their contact angle hysteresis. Figure 6c shows the contact angle hysteresis for flat PDMS (PDMS sheet without roughness), PDMS sheet with only nanoscale roughness micron-scale wrinkles and dual-scale wrinkles. The result indicates that contact angle hysteresis is higher (~60°) for flat PDMS and PDMS sheet with only nano- and micron-scale roughness as compared to dual-scale wrinkles (~40°). This is because on PDMS sheets with only micron- and nanoscale roughness, water drops go into Wenzel wetting state whereas on dual-scale wrinkles, the drops are in the Cassie impregnating state. The contact area between the drop and surface is less in the Cassie impregnating state compare to Wenzel state. As adhesion or stickiness is proportional to the contact area, contact angle hysteresis on dual-scale wrinkles show smaller value compared to other

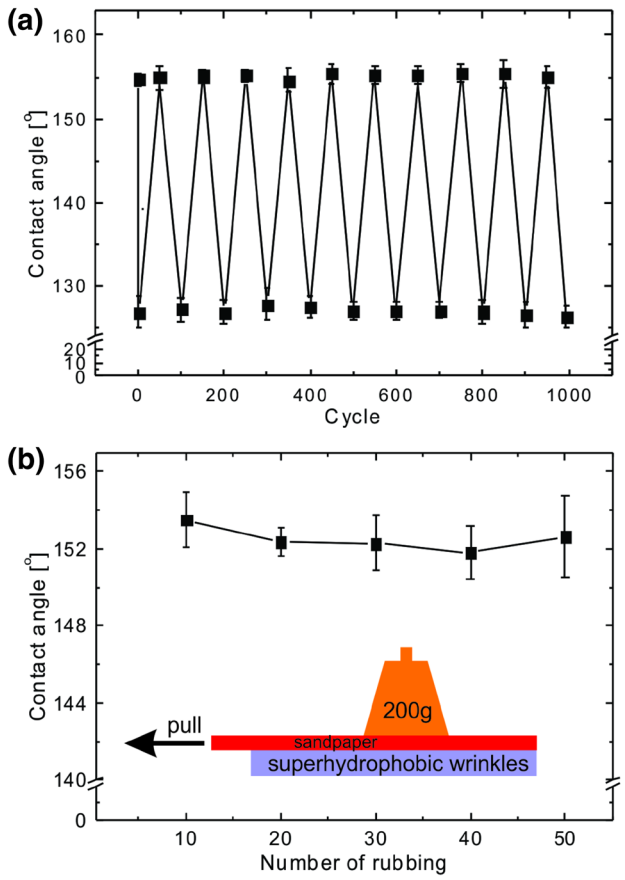


**Fig. 7** **a** Reversible transition of contact angle between Cassie to Wenzel state with corresponding applied strain between 0 and 60%. **b** Contact angle as a function of number of rubbing and inside schematic shows the procedure of rubbing

scale rough surfaces. The dual-scale superhydrophobic wrinkles are found very robust against mechanical strain. Switching the wetting behavior with mechanical stretching and relaxing is very robust as the fabricated samples do not show any deterioration even up to 1000 cycles. Mechanical robustness of superhydrophobic wrinkles was verified by measuring water contact angle as well as the surface morphology with scanning electron microscope.

Figure 7a shows the water contact angles on stretched and relaxed dual-scale wrinkles between 0 and 60% apply strains for multiple cycles showing almost constant values of 154°–128° contact angles, respectively. In the relaxed state (0% strain) and completely stretched state (60% strain), water contact angle changes from 154°–128°, respectively. To demonstrate the stability against mechanical damage (wear and tear), the dual-scale wrinkles were tested by rubbing them with 1200 grit sandpapers (3 M, mean particle size 15 μm) loaded with 200 g weight pulled with 4 mm/s speed as shown in Fig. 7b (see supporting movie MovieS4). The rubbed samples were tested for their wetting behavior and its tunability and morphology after multiple rubbing cycles. The dual-scale wrinkles showed excellent robustness against the mechanical damage testing as no deterioration in any of its characteristics could be observed. Furthermore, the chemical stability of the dual-scale wrinkles in the presence of concentrated acid, base or organic solvents (toluene), is analyzed by measuring the water contact angles before and after dipping them in respective liquids for 5 min. All the samples retained their superhydrophobicity after being treated with concentrated acid, base or organic solvent (see supporting information FigureS1). Hence, single-component PDMS-based dual-scale superhydrophobic wrinkles show robust, durable and excellent superhydrophobic behavior.

## 4 Conclusion

In conclusion, we have successfully fabricated single-component, pure PDMS-based superhydrophobic wrinkles having dual-scale roughness; micron scale due to wrinkles and nanoscale due to replica molding from a nano-master. Due to the elastic nature of PDMS, wrinkles show tunable wetting behavior as a function of applied mechanical strain. In addition, due to use of pure PDMS to create micro- and nanoscale roughness, dual-scale wrinkles show excellent robustness against mechanical damage. Due to underlying topography, as prepared wrinkles, with only micron-scale roughness, show anisotropic wetting behavior with two different contact angles along two different directions. Hydrophobic wrinkles are prepared by taking the replica of the as prepared wrinkles and they do not show anisotropic wetting behavior due to high contact angle. Similarly, superhydrophobic wrinkles also do not show wetting anisotropicity. Water contact angles on such surfaces can be reversibly tuned from 155° to 125° by applying 60% strain. The superhydrophobic state of the dual-scale wrinkles correspond to the Cassie impregnating wetting state due to which water drops on them gets stuck and do not move at all. Also, the dual-scale superhydrophobic wrinkles show excellent robustness against mechanical and chemical damages.

**Acknowledgements** This research work was supported by DST, New Delhi through its Unit of Excellence on Soft Nanofabrication at IIT Kanpur.

**Funding** Funding was provided by Science and Engineering Research Board (NanoMission).

## References

1. Z. Hu, Y. Chen, C. Wang, Y. Zheng, Y. Li, Polymer gels with engineered environmentally responsive surface patterns. Nature **393**, 149–152 (1998)

2. D.E. Kataoka, S.M. Troian, Patterning liquid flow on the microscopic scale. Nature **402**, 794–797 (1999)
3. M. Fujihira, Y. Tani, M. Furugori, U. Akiba, Y. Okabe, Chemical force microscopy of self-assembled monolayers on sputtered gold films patterned by phase separation. Ultramicroscopy **86**, 63–73 (2001)
4. J. Taktikos, H. Behringer, Dry and wet interfaces: influence of solvent particles on molecular recognition. Phys. Rev. E **79**, 041908 (2009)
5. A. Majumder, A. Sharma, A. Ghatak, A bioinspired wet/dry microfluidic adhesive for aqueous environments. Langmuir **26**, 521–525 (2010)
6. P.G. de Gennes, Wetting: statics and dynamics. Rev. Mod. Phys. **57**, 827–863 (1985)
7. T. Sun, L. Feng, X. Gao, L. Jiang, Bioinspired surfaces with special wettability. Acc. Chem. Res. **38**, 644–652 (2005)
8. A. Malijevský, Does surface roughness amplify wetting? J. Chem. Phys. **141**, 184703 (2014)
9. D. Quere, Wetting and roughness. Annu. Rev. Mater. Res. **38**, 71–99 (2008)
10. S. Herminghaus, Roughness-induced non-wetting. Europhys. Lett. **52**, 165–170 (2000)
11. C. Huh, S.G. Mason, Effects of surface roughness on wetting (theoretical). J. Colloid Interface Sci. **60**, 11–38 (1977)
12. S. Wang, L. Jiang, Definition of superhydrophobic states. Adv. Mater. **19**, 3423–3424 (2007)
13. B. Cortese, S. D'Amone, M. Manca, I. Viola, R. Cingolani, G. Gigli, Superhydrophobicity due to the hierarchical scale roughness of PDMS surfaces. Langmuir **24**, 2712–2718 (2008)
14. M. He, H. Li, J. Wang, Y. Song, Superhydrophobic surface at low surface temperature. Appl. Phys. Lett. **98**, 093118 (2011)
15. Y. Li, S. Dai, J. John, K.R. Carter, Superhydrophobic surfaces from hierarchically structured wrinkled polymers. ACS Appl. Mater. Interfaces **5**, 11066–11073 (2013)
16. J. Long, P. Fan, D. Gong, D. Jiang, H. Zhang, L. Li, M. Zhong, Superhydrophobic surfaces fabricated by femtosecond laser with tunable water adhesion: from lotus leaf to rose petal. ACS Appl. Mater. Interfaces **7**, 9858–9865 (2015)
17. M. Yamamoto, N. Nishikawa, H. Mayama, Y. Nonomura, S. Yokojima, S. Nakamura, K. Uchida, Theoretical explanation of the lotus effect: superhydrophobic property changes by removal of nanostructures from the surface of a lotus leaf. Langmuir **31**, 7355–7363 (2015)
18. S.K. Ujjain, P.K. Roy, S. Kumar, S. Singha, K. Khare, Uniting superhydrophobic, superoleophobic and lubricant infused slippery behavior on copper oxide nano-structured substrates. Sci. Rep. **6**, 35524 (2016)
19. A. Fernández, A. Francone, L.H. Thamdrup, A. Johansson, B. Bilenberg, T. Nielsen, M. Guttmann, C.M. Sotomayor Torres, N. Kehagias, Design of hierarchical surfaces for tuning wetting characteristics. ACS Appl. Mater. Interfaces **9**, 7701–7709 (2017)
20. X. Hong, X. Gao, L. Jiang, Application of superhydrophobic surface with high adhesive force in no lost transport of superparamagnetic microdroplet. J. Am. Chem. Soc. **129**, 1478–1479 (2007)
21. B. Bhushan, E.K. Her, Fabrication of superhydrophobic surfaces with high and low adhesion inspired from rose petal. Langmuir **26**, 8207–8217 (2010)
22. L. Gao, T.J. McCarthy, The "lotus effect" explained: two reasons why two length scales of topography are important. Langmuir **22**, 2966–2967 (2006)
23. M.K. Dawood, H. Zheng, T.H. Liew, K.C. Leong, Y.L. Foo, R. Rajagopalan, S.A. Khan, W.K. Choi, Mimicking both petal and lotus effects on a single silicon substrate by tuning the wettability of nanostructured surfaces. Langmuir **27**, 4126–4133 (2011)
24. L. Feng, Y. Zhang, J. Xi, Y. Zhu, N. Wang, F. Xia, L. Jiang, Petal effect: a superhydrophobic state with high adhesive force. Langmuir **24**, 4114–4119 (2008)
25. K.J. Park, J.H. Park, J.H. Huh, C.H. Kim, D.H. Ho, G.H. Choi, P.J. Yoo, S.M. Cho, J.H. Cho, S. Lee, Petal-inspired diffractive grating on a wavy surface: deterministic fabrications and applications to colorizations and LED devices. ACS Appl. Mater. Interfaces **9**, 9935–9944 (2017)
26. S.-Y. Chou, C.-C. Yu, Y.-T. Yen, K.-T. Lin, H.-L. Chen, W.-F. Su, Romantic story or Raman scattering? Rose petals as ecofriendly, low-cost substrates for ultrasensitive surface-enhanced Raman scattering. Anal. Chem. **87**, 6017–6024 (2015)
27. D. Zheng, Y. Jiang, W. Yu, X. Jiang, X. Zhao, C.H. Choi, G. Sun, Salvinia-effect-inspired "sticky" superhydrophobic surfaces by meniscus-confined electrodeposition. Langmuir **33**, 13640–13648 (2017)
28. M. Jin, X. Feng, L. Feng, T. Sun, J. Zhai, T. Li, L. Jiang, Superhydrophobic aligned polystyrene nanotube films with high adhesive force. Adv. Mater. **17**, 1977–1981 (2005)
29. W. Tong, D. Xiong, T. Tian, Y. Liu, Superhydrophobic surface on aeronautical materials via the deposition of nanoparticles and a PDMS seal. Appl. Phys. A Mater. Sci. Process. **125**, 177 (2019)
30. S. Dai, Y. Zhu, Y. Gu, Z. Du, Biomimetic fabrication and photoelectric properties of superhydrophobic ZnO nanostructures on flexible PDMS substrates replicated from rose petal. Appl. Phys. A Mater. Sci. Process. **125**, 138 (2019)
31. S.S. Sanjay, S. Latthea, R.S. Sutar, V.S. Kodag, A.K. Bhosale, A.M. Kumar, K.K. Sadasivuni, R. Xinga, S. Liu, Self-cleaning superhydrophobic coatings: potential industrial applications. Prog. Org. Coat. **128**, 52–58 (2019)
32. R. Taurino, E. Fabbri, D. Pospiech, A. Synytska, M. Messori, Preparation of scratch resistant superhydrophobic hybrid coatings by sol–gel process. Prog. Org. Coat. **77**, 1635–1641 (2014)
33. S.-A. Seyedmehdi, R. Vrckovnik, A. Amirfazli, Robust superhydrophobic coatings from modified siloxane resin. Surf. Innov. **5**, 203–210 (2017)
34. D. Zhanga, L. Lia, Y. Wua, B. Zhue, H. Song, One-step method for fabrication of bioinspired hierarchical superhydrophobic surface with robust stability. Appl. Surf. Sci. **473**, 493–499 (2019)
35. A. Bake, N. Merah, A. Matin, M. Gondal, T. Qahtan, N. Abu-Dheir, Preparation of transparent and robust superhydrophobic surfaces for selfcleaning applications. Prog. Org. Coat. **122**, 170–179 (2018)
36. N. Wang, D. Xiong, Y. Deng, Y. Shi, K. Wang, Mechanically robust superhydrophobic steel surface with anti-icing, UV-durability, and corrosion resistance properties. ACS Appl. Mater. Interfaces **7**, 6260–6272 (2015)
37. C. Hu, W. Chen, T. Li, Y. Ding, H. Yang, S. Zhao, S.A. Tsiwah, X. Zhao, Y. Xie, Constructing non-fluorinated porous superhydrophobic $SiO_2$-based films with robust mechanical properties. Colloids Surf. A **551**, 65–73 (2018)
38. X. Deng, L. Mammen, Y. Zhao, P. Lellig, K. Müllen, C. Li, H.-J. Butt, D. Vollmer, Transparent, thermally stable and mechanically robust superhydrophobic surfaces made from porous silica capsules. Adv. Mater. **23**, 2962–2965 (2011)
39. P. Wang, J. Liu, W. Chang, X. Fan, C. Li, Y. Shi, A facile cost-effective method for preparing robust self-cleaning transparent superhydrophobic coating. Appl. Phys. A **1222**, 916 (2016)
40. P. Goel, S. Kumar, J. Sarkar, J.P. Singh, Mechanical strain induced tunable anisotropic wetting on buckled PDMS silver nanorods arrays. ACS Appl. Mater. Interfaces **7**, 8419–8426 (2015)
41. P.C. Lin, S. Yang, Mechanically switchable wetting on wrinkled elastomers with dual-scale roughness. Soft Matter **5**, 1011–1018 (2009)

42. R. Pant, S. Singha, A. Bandyopadhyay, K. Khare, Investigation of static and dynamic wetting transitions of UV responsive tunable wetting surfaces. Appl. Surf. Sci. **292**, 777–781 (2014)
43. M. Sha, D. Niu, Q. Dou, G. Wu, H. Fang, J. Hu, Reversible tuning of the hydrophobic–hydrophilic transition of hydrophobic ionic liquids by means of an electric field. Soft Matter **7**, 4228–4233 (2011)
44. E. Stratakis, A. Mateescu, M. Barberoglou, M. Vamvakaki, C. Fotakis, S.H. Anastasiadis, From superhydrophobicity and water repellency to superhydrophilicity: Smart polymer-functionalized surfaces. Chem. Commun. **46**, 4136–4138 (2010)
45. F. Xia, L. Feng, S. Wang, T. Sun, W. Song, W. Jiang, L. Jiang, Dual-responsive surfaces that switch between superhydrophilicity and superhydrophobicity. Adv. Mater. **18**, 432–436 (2006)
46. S. Zhao, H. Xia, D. Wu, C. Lv, Q.D. Chen, K. Ariga, L.Q. Liu, H.B. Sun, Mechanical stretch for tunable wetting from topological PDMS film. Soft Matter **9**, 4236–4240 (2013)
47. J.Y. Chung, J.P. Youngblood, C.M. Stafford, Anisotropic wetting on tunable micro-wrinkled surfaces. Soft Matter **3**, 1163–1169 (2007)
48. K. Khare, J. Zhou, S. Yang, Tunable open-channel microfluidics on soft poly(dimethylsiloxane) (PDMS) substrates with sinusoidal grooves. Langmuir **25**, 12794–12799 (2009)
49. S. Yang, K. Khare, P.C. Lin, Harnessing surface wrinkle patterns in soft matter. Adv. Funct. Mater. **20**, 2550–2564 (2010)
50. G. Carbone, L. Mangialardi, Hydrophobic properties of a wavy rough substrate. Eur. Phys. J. E Soft Matter Biol. Phys. **16**, 67–76 (2005)
51. N.T.P. Nguyen, Y. Coffinier, V. Thomy, R. Boukherroub, Fabrication of silicon nanostructures using metal-assisted etching in $NaBF_4$. Phys. Status Solidi A **210**, 2178–2182 (2013)
52. Y.-J. Fu, H.-Z. Qui, K.-S. Liao, S.J. Lue, C.-C. Hu, K.-R. Lee, J.-Y. Lai, Effect of UV-ozone treatment on poly(dimethylsiloxane) membranes: surface characterization and gas separation performance. Langmuir **26**, 4392–4399 (2009)
53. S. Vajpayee, K. Khare, S. Yang, C.-Y. Hui, A. Jagota, Adhesion selectivity using rippled surfaces. Adv. Funct. Mater. **21**, 547–555 (2011)
54. H. Jiang, D.Y. Khang, J. Song, Y. Sun, Y. Huang, J.A. Rogers, Finite deformation mechanics in buckled thin films on compliant supports. Proc. Natl. Acad. Sci. USA **104**, 15607–15612 (2007)
55. A.L. Volynskii, S. Bazhenov, O.V. Lebedeva, N.F. Bakeev, Mechanical buckling instability of thin coatings deposited on soft polymer substrates. J. Mater. Sci. **35**, 547–554 (2000)